Int. J. Heat Mass Transfer. Vol. 35, No. 5, pp. 1181–1195, 1992
Printed in Great Britain

0017–9310/92 $5.00 + 0.00

Solution of Stefan problems imposed with cyclic temperature and flux boundary conditions

CHANG-YONG CHOI and C. K. HSIEH
Mechanical Engineering Department, University of Florida, Gainesville, FL 32611, U.S.A.

(*Received* 5 *December* 1990 *and in final form* 6 *May* 1991)

Abstract—Stefan problems imposed with cyclic temperature and flux boundary conditions are solved by using source and sink methods. A source front is associated with a moving freeze front while a sink front is associated with a moving melt front. The solution is expressed in a set of coupled integrodifferential equations, which are solved numerically for interface positions, temperature profiles, and cumulative and instantaneous heat storage and release. The solution methods have been shown to be unique, convergent, stable, and accurate. While they are used to test one cycle each of the temperature and flux conditions, the developed methods are general and applicable to multiple cycles. The numerical results reveal interesting phenomena not previously reported in the literature. Their relevance to energy storage and material processing and treatment is also covered.

INTRODUCTION

CYCLIC heat injection to and rejection from a phase-change material involves a multiphase, simultaneous melting and solidification process, which finds applications in energy storage, chemical reaction, and material and food processing and treatment, among others. Analysis of the heat transfer in this process calls for the study of a moving boundary problem or a Stefan problem, which is difficult to solve because the boundary of the problem domain is imposed with a time-variant cyclic condition. During the heating phase of the cycle, the medium melts and the melting front moves from the surface to the interior of the body. Next, during the cooling phase of the cycle, the melted region near the surface re-freezes and a freezing front also appears. There are two phase-change fronts in the medium and whether the second freeze front is able to catch up the first melt front and how the heat is stored and released in different phases of the medium depends greatly on the Stefan number and on the conditions that are imposed on the surface. It is impossible to solve this problem exactly [1–9]; only approximate solutions are possible and the problem poses a real challenge to accurate analysis.

Of the approximate solutions developed for the analysis of the Stefan problem, power series and polynomials of complimentary error functions have been used to represent the temperature and interface position for boundaries imposed with Neumann and Robin conditions [10–14]. They are known as the power series methods and are accurate at small time; at large time, more terms are necessary for the expansions, and the methods lose their appeal. Stefan problems can also be solved by using asymptotic expansions, which use quasi-steady and quasi-stationary solutions for limits. Primarily a perturbation technique, the method provides a means for analysis of the singularity associated with phase degeneration if singular perturbation is employed. However, considerable effort is necessary in determining higher order terms, a drawback greatly limiting its usefulness [15–22].

For materials with equal solid and liquid properties, a heat source can be used to characterize a freezing front in the analysis of a solidification process [23]. Generalization to unequal material properties has been attempted by Kolodner [24] and Tao [25]. The solution of the moving boundary characteristic of the Stefan problem can also be simplified by embedding the problem domain in a large space with fixed boundaries [24, 26]. These methods lead to the solution of integrodifferential equations. An alternative approach akin to the embedding method is the use of coordinate transformation, which, by scaling space and time, permits simplification of the solution by working in a fixed domain [27–34]. The transformation also enables the improvement of the accuracy of solution [9, 35]. Another popular approach is the use of the integral method, which unlike the enthalpy method that works well for phase change over an extended zone, is easy to apply yet yields results that are reasonably accurate over a wide range of time [3, 36–39]. Recently, Stefan problems have been solved as a system of integral equations [40, 41]. Fourier series have been used for spatial temperature expansions, thus leading to the solution of a set of ordinary differential equations in time [42]. Stefan problems have also been solved as an inverse problem [43]. In purely numerical efforts, the modern trend is to use boundary element methods

NOMENCLATURE

c	specific heat
e	infinitesimal quantity
F	imposed temperature condition
G	imposed flux condition, or Green's function
H	circumflexed Heaviside function
i	index
k	thermal conductivity
L	latent heat
m	parameter for mode of heat input
N	upper limit for time index
Q	total heat flux
q	instantaneous heat flux
R	interface position
s	interface speed
T	temperature
t	time
x	position.

Greek symbols

α	thermal diffusivity
δ	Dirac delta function
ξ	dummy variable for position
ρ	density
τ	dummy variable for time.

Subscripts

a, b, c	regions
m	phase change
N_1, N_2	upper limits for time index in the first and second stages
n	time index
t	transition time
0	temperature equation (24)
1, 2	melt and freeze fronts, or first and second stages.

in place of finite difference and finite element methods in the solution of Stefan problems [44–49].

A close examination of the solution methods documented in the literature reveals that there is a lack of accurate methods for the solution of Stefan problems imposed with cyclic temperature and flux conditions. It is expected that, for the methods to be useful for the present problem, the solution must be accurate not only at small time but large time as well. The methods must be general so that multiphase can be analyzed without reformulations of the problem. Furthermore, the solution techniques must be simple and permit the development of algorithms adaptable to both temperature and flux conditions. It is with these goals in mind this paper is offered.

ANALYSIS

The system for investigation is shown in Fig. 1, where a one-dimensional semi-infinite medium with equal solid and liquid properties is considered. The material is initially at its phase-change temperature—there is no subcooling or superheating in the medium. Once heat is supplied to or removed from the surface, a phase-change front emerges as shown by the dashed lines marked as $R_1(t)$. This front moves from left to right and divides the domain into two regions; the one ahead of the front is called a, that behind it is called b. Then using the heat cycle illustrated in Fig. 2, the first stage temperature, covering the period from time zero to the time when the surface re-freezes due to heat removal during the second half of the cycle, can be obtained by solving the following problem.

First stage problem

Region b

Governing equation

$$\frac{\partial^2 T_b}{\partial x^2} = \frac{1}{\alpha}\frac{\partial T_b}{\partial t}, \quad T_b(x,t), \quad \begin{matrix} 0 < x < R_1(t) \\ t_1 \geqslant t > 0 \end{matrix} \tag{1}$$

Boundary condition

$$T_b(0,t) = F(t) \quad \text{or} \quad -k\frac{\partial T_b(0,t)}{\partial x} = G(t) \tag{2a,b}$$

Region a

$$T_a(x,t) = T_m = 0, \quad \begin{matrix} R_1(t) \leqslant x < \infty \\ t \geqslant 0 \end{matrix} \tag{3}$$

Interface conditions

$$T_b(R_1(t),t) = 0 = T_m \tag{4}$$

$$-k\frac{\partial T_b(R_1(t),t)}{\partial x} = \rho L\frac{dR_1}{dt} \tag{5}$$

$$R_1(0) = 0. \tag{6}$$

Here all notations have their usual meaning. Notice that (2a,b) represent time-variant temperature and flux conditions. Equation (5) is valid for the heat cycle shown in Fig. 2. The sign on the left hand side of (5) would be changed if the heat-out phase (HOP) precedes the heat-in phase (HIP).

Once the surface is cooled below freezing point, the second stage starts. A freezing front emerges, which, together with the melting front earlier, divides the medium into three regions (see lower half of Fig. 2).

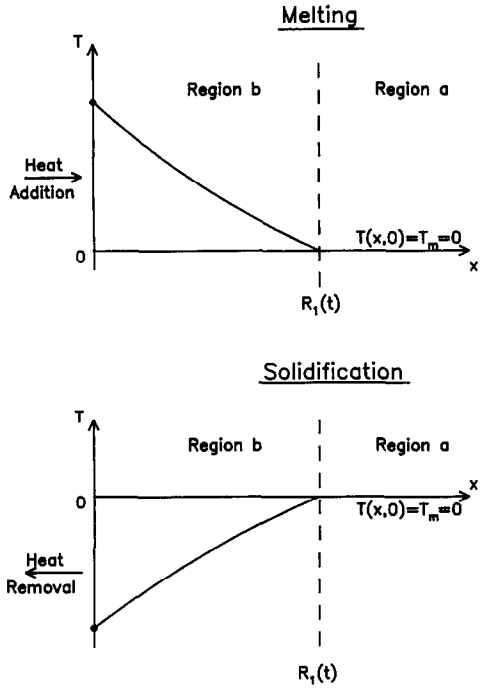

FIG. 1. Coordinates used for phase change analysis.

Temperatures in these regions can be solved by using the following equations.

Second stage problem

Region c

Governing equation

$$\frac{\partial^2 T_c}{\partial x^2} = \frac{1}{\alpha}\frac{\partial T_c}{\partial t}, \quad T_c(x,t), \quad \begin{matrix} 0 < x < R_2(t) \\ t > t_i \end{matrix} \tag{7}$$

Boundary condition

$$T_c(0,t) = F(t) \quad \text{or} \quad -k\frac{\partial T_c(0,t)}{\partial x} = G(t) \tag{8a,b}$$

Region b

Governing equation

$$\frac{\partial^2 T_b}{\partial x^2} = \frac{1}{\alpha}\frac{\partial T_b}{\partial t}, \quad T_b(x,t), \quad \begin{matrix} R_2(t) < x < R_1(t) \\ t > t_i \end{matrix} \tag{9}$$

Initial condition

$$T_b(x,t) = T_b(x,t_i) \quad \text{for } t = t_i \tag{10}$$

Region a

$$T_a(x,t) = T_m = 0, \quad \begin{matrix} R_1(t) \leqslant x < \infty \\ t \geqslant t_i \end{matrix} \tag{11}$$

Interface conditions

$$T_c(R_2(t),t) = 0 = T_m \tag{12}$$

$$-k\frac{\partial T_b(R_2(t),t)}{\partial x} + k\frac{\partial T_c(R_2(t),t)}{\partial x} = \rho L\frac{dR_2}{dt} \tag{13}$$

$$R_2(t_i) = 0 \tag{14}$$

$$T_b(R_1(t),t) = 0 = T_m \tag{15}$$

$$-k\frac{\partial T_b(R_1(t),t)}{\partial x} = \rho L\frac{dR_1}{dt}. \tag{16}$$

Again signs on the left hand sides of (13) and (16) would be changed if HOP precedes HIP.

A source and sink method is developed for the solution of the present problem. This method is an extension of the Lightfoot method, which was originally developed for the solution of a solidification problem of equal solid and liquid properties and imposed with a constant temperature condition [23]. For the problem at hand, a heat sink is postulated to associate with a melting front while a heat source is associated with a freezing front. Then, as in the Lightfoot method, the original problem in multiple regions can be consolidated into a single problem in a big domain, which is divided into separate regions by the moving source and sink fronts. One temperature will then be derived, and whether it is in the solid or liquid region depends on the position that is

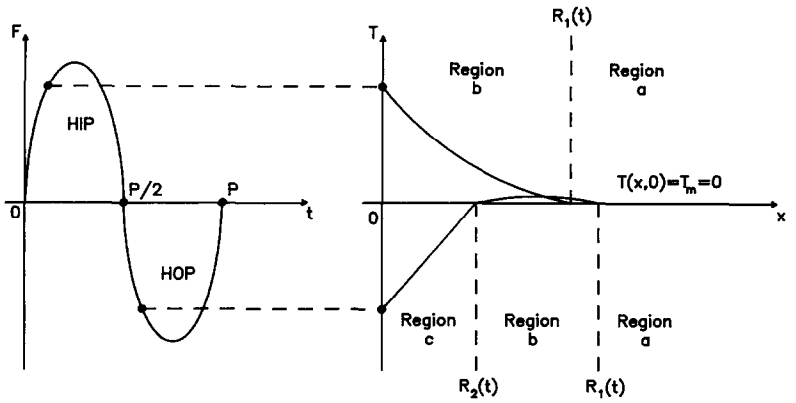

FIG. 2. Regions of domain formed by imposition of cyclic temperature conditions.

assigned in the temperature equation. The original problems in two stages are also incorporated into one so that a single equivalent problem is formulated. A general temperature can be derived as follows.

General equivalent problem

Governing equation

$$\frac{\partial^2 T}{\partial x^2} - \frac{\rho L}{k}\frac{\mathrm{d}R_1}{\mathrm{d}t}\delta_1[x-R_1(t)] + \frac{\rho L}{k}\frac{\mathrm{d}R_2}{\mathrm{d}t}\delta_2[x-R_2(t)] = \frac{1}{\alpha}\frac{\partial T}{\partial t} \quad (17)$$

Boundary condition

$$T(0,t) = F(t) \quad \text{or} \quad -k\frac{\partial T(0,t)}{\partial x} = G(t) \quad (18a,b)$$

Interface conditions

$$T(R_1(t),t) = 0 = T_m \quad (19)$$

$$T(R_2(t),t) = 0 = T_m \quad (20)$$

Initial conditions

$$T(x,0) = T_m = 0 \quad (21)$$

$$T(x,t) = T_1(x,t_t) \quad \text{for } t = t_t. \quad (22)$$

It is noted that, when using the general problem above to solve the first stage problem, δ_2 in (17) and equations (20) and (22) must be deleted. On the other hand, when using it to solve the second stage problem, (21) must be deleted. In addition, the signs preceding δ_1 and δ_2 must be interchanged if HOP precedes HIP. With these minor changes, the general problem can be shown to be reducible to (1)–(16). For example, setting $x \neq R_1(t)$ and $R_2(t)$ reduces (17) to (1), (7) and (9). Also, integrating (17) from $R_2(t)-e$ to $R_2(t)+e$ and forcing the e to be zero in a limiting process reduces (17) to (13). Other equivalences follow immediately.

The first stage temperature can be obtained by solving the revised versions of (17)–(19) and (21). Green's function method can be used and the temperature derived as

$$T_1(x,t) = T_0(x,t) - \frac{L}{c}\int_{\tau=0}^{t}\frac{\mathrm{d}R_1(\tau)}{\mathrm{d}\tau}G(x,t|R_1(\tau),\tau)\,\mathrm{d}\tau \quad (23)$$

where

$$T_0(x,t) = \sqrt{\left(\frac{\alpha}{\pi}\right)}\int_{\tau=0}^{t}\frac{E(\tau)}{(t-\tau)^{1/2}}\exp\left[-\frac{x^2}{4\alpha(t-\tau)}\right]\mathrm{d}\tau \quad (24)$$

$$E(\tau) = \begin{cases} \dfrac{x}{2\alpha}\dfrac{F(\tau)}{t-\tau} & F(t) \\ \dfrac{1}{k}G(\tau) & G(t) \end{cases} \quad \text{for} \quad \text{imposed at } x = 0 \quad (25)$$

$$G(x,t|x',\tau) = \frac{1}{\sqrt{(4\pi\alpha(t-\tau))}} \times \left\{\exp\left[-\frac{(x-x')^2}{4\alpha(t-\tau)}\right] \pm \exp\left[-\frac{(x+x')^2}{4\alpha(t-\tau)}\right]\right\}. \quad (26)$$

Here the plus and minus signs in the Green's function in (26) are to be used when flux and temperature conditions, respectively, are imposed on the boundary.

Equation (23) can be used to derive the interface position $R_1(t)$ by setting $x = R_1(t)$ and $T_1(R_1(t),t) = 0$ as

$$T_0(R_1(t),t) = \frac{L}{c}\int_{\tau=0}^{t}\frac{\mathrm{d}R_1(\tau)}{\mathrm{d}\tau}G(R_1(t),t|R_1(\tau),\tau)\,\mathrm{d}\tau. \quad (27)$$

Likewise, setting t to t_t in (23) yields

$$T_1(x,t_t) = T_0(x,t_t) - \frac{L}{c}\int_{\tau=0}^{t_t}\frac{\mathrm{d}R_1(\tau)}{\mathrm{d}\tau}G(x,t_t|R_1(\tau),\tau)\,\mathrm{d}\tau \quad (28a)$$

which is to be used for the initial condition for the second stage temperature derived later.

It is clear that, for a cyclic temperature imposed on the surface, $t_t = P/2$, where P stands for the period of the cycle. For this temperature condition, although $T_1(0,t_t)$ is zero, $T_1(x,t_t)$ is not for $x > 0$. On the other hand, for a cyclic heat flux imposed on the surface, t_t must be determined by solving the following equation implicitly:

$$T_m = 0 = T_0(0,t_t) - \frac{L}{c}\int_{\tau=0}^{t_t}\frac{\mathrm{d}R_1(\tau)}{\mathrm{d}\tau}G(0,t_t|R_1(\tau),\tau)\,\mathrm{d}\tau. \quad (28b)$$

For the flux condition imposed on the surface, energy can be stored in the form of sensible heat. The time t_t is thus greater than $P/2$, as will be shown later.

The second stage temperature can be derived by solving (17)–(20) and (22). Again the Green's function method is used and the solution derived as

$$T_2(x,t) = T_0(x,t-t_t) + \int_{x'=0}^{\infty}T_1(x',t_t)G(x,t-t_t|x',0)\,\mathrm{d}x' + \frac{L}{c}\int_{\tau=0}^{t-t_t}\left[-\frac{\mathrm{d}R_1(\tau+t_t)}{\mathrm{d}\tau}G(x,t-t_t|R_1(\tau+t_t),\tau) + \frac{\mathrm{d}R_2(\tau+t_t)}{\mathrm{d}\tau}G(x,t-t_t|R_2(\tau+t_t),\tau)\right]\mathrm{d}\tau. \quad (29)$$

Here the first term on the right hand side can be obtained by referring to (24), in which t is changed to $t-t_t$ and $F(\tau)$ and $G(\tau)$ are changed to $F(\tau+t_t)$ and $G(\tau+t_t)$, respectively; the other τ in (24) remain unchanged.

Equation (29) as derived cannot be used for general solution; the double integral implicitly contained in the second term on the right hand side must be integrated and, following a lengthy procedure, two identities are derived as follows:

$$\int_{x'=0}^{\infty} T_0(x', t_i)G(x, t-t_i|x', 0)\,dx'$$

$$= \sqrt{\left(\frac{\alpha}{\pi}\right)}\int_{\tau=0}^{t_i}\frac{E(\tau)}{(t-\tau)^{1/2}}\exp\left[-\frac{x^2}{4\alpha(t-\tau)}\right]d\tau \quad (30)$$

$$\int_{\tau=0}^{t-t_i}\left[-\frac{dR_1(\tau+t_i)}{d\tau}G(x, t-t_i|R_1(\tau+t_i), \tau)\right]d\tau$$

$$-\int_{x'=0}^{\infty}\int_{\xi=0}^{t_i}\frac{dR_1(\xi)}{d\xi}G(x', t_i|R_1(\xi), \xi)$$

$$\times G(x, t|x', t_i)\,d\xi\,dx'$$

$$= -\int_{\tau=0}^{t}\frac{dR_1(\tau)}{d\tau}G(x, t|R_1(\tau), \tau)\,d\tau \quad (31)$$

where Green's function has been given by the general expression in (26).

Using (30) and (31) in (29) and changing time frames yields

$$T_2(x, t) = T_0(x, t)$$

$$+\frac{L}{c}\int_{\tau=0}^{t}\left(-\frac{dR_1(\tau)}{d\tau}\right)G(x, t|R_1(\tau), \tau)\,d\tau$$

$$+\frac{L}{c}\int_{\tau=t_i}^{t}\left(+\frac{dR_2(\tau)}{d\tau}\right)G(x, t|R_2(\tau), \tau)\,d\tau. \quad (32)$$

This equation can be used to determine the second-stage temperature in a phase-change material whose boundary is imposed with a cyclic temperature or flux condition as shown in Fig. 2.

Equation (32) can also be extended for any cyclic temperature as follows [49]:

$$T(x, t) = T_0(x, t)+\frac{L}{c}\sum_{i=1}^{I}\left\{\hat{H}\left(t-\frac{(i-1)P}{2}\right)\right.$$

$$\left.\times\int_{\tau=(i-1)P/2}^{t}(-1)^{m+i-1}\frac{dR_i(\tau)}{d\tau}G(x, t|R_i(\tau), \tau)\,d\tau\right\} \quad (33)$$

where the parameter m is used to control the mode of heat input

$$m = \begin{cases}1 & \text{for HIP at } t = 0^+\\ 2 & \text{for HOP at } t = 0^+\end{cases} \quad (34)$$

and I denotes the number of phase-change fronts. $\hat{H}$ is used to represent the circumflexed Heaviside function defined as

$$\hat{H}\left(t-\frac{(i-1)P}{2}\right)$$

$$= \begin{cases}1 & t > \dfrac{(i-1)P}{2}\\ \text{for} & \\ 0 & t \leqslant \dfrac{(i-1)P}{2}\end{cases} \quad i = 1, 2, \ldots \quad (35)$$

With the use of the Heaviside function, equation (33) holds for all time. Also notice that, because of the format in which (33) is written, multiple phase problems can be analyzed with this equation. As for cyclic flux conditions, $(i-2)P/2$ in (33) and (35) will be changed to t_i as explained in (28b) and in more detail later.

A short note is in order to discuss the temperature obtained. Since no assumptions have been made in the course of derivation, equation (33) is exact but expressed in an integrodifferential form. It is unexpected that the Green function method, which is strictly valid for the solution of linear problems, has been used here to solve a nonlinear problem. This is possible because the nonlinearity in the Stefan problem is confined in the interface conditions. For the present source-and-sink method of solution, the interface positions can be determined by setting the left hand side of (33) to zero and solving it for $R_i(t)$ as in (27). Thus the interface positions are solved by using a separate equation, which is characteristically nonlinear, a result enabling the use of a linear method to solve nonlinear problems [9].

The format of equation (33) is also worthy of note. It is valid for any cyclic temperature or flux condition imposed on the boundary. Notice that changing the boundary condition only changes the sign in the Green function. The only major change due to the boundary condition is the first term on the right hand side of (33), which, as shown in (24), can be integrated in closed form once the cyclic condition is specified [49–51]. Clearly $dR_i(\tau)/d\tau$ is unknown in (33), yet if moved out of the integral under which it is located—local linearization—the Green function can be integrated if the R_i is related to $dR_i(\tau)/d\tau$ in an iteration process. These features permit the planning of a solution strategy adaptable to different boundary conditions [52]; they also provide the basis for the development of numerical solution as described in the next section.

NUMERICAL SOLUTION

It is well known that the Stefan problem in an extended domain cannot be solved exactly other than with a constant temperature condition imposed on the boundary. For the problem at hand, the surface is exposed to a cyclic condition; the interface positions must be solved numerically.

The numerical solution is effected by using local linearization; the $dR_i(\tau)/d\tau$ in (33) is moved out of the integral. Thus for $0 < t \leqslant t_1$ with HIP preceding HOP, i and m in (33) are set to unity. The interface positions in the first stage are determined by setting x to $R_1(t)$ and $T(R_1(t), t)$ to 0 in (33) as

$$\sum_{n=1}^{N_1} \left\{ \frac{dR_1(t_n^-)}{dt} \int_{\tau=t_{n-1}}^{t_n} G(R_1(t_{N_1}), t_{N_1} | R_1(\tau), \tau)\, d\tau \right\} = \frac{c}{L} T_0(R_1(t_{N_1}), t_{N_1}) \quad (36)$$

where $t_0 = 0$; $R_1(0) = 0$; $N_1 = 1, 2, \ldots, N_1$; $t_{N_1} \leqslant t_1$. Moving the $dR_i(\tau)/d\tau$ out of the integral is inspired by the fact that, within small time intervals, the position curve can be approximated as linear. For the Stefan problem, the curvature of the interface position usually lies in a small time range, as shown in Fig. 3. Then, only over this range, the removal of the differential will cause a slight error in the solution of the interface position, yet such error can still be reduced by taking small time increments. Better still, the left hand side of (36) consists of a summation. Since the curvature of R_1 is confined in a small time range, the accurate terms in the summation easily outnumber the inaccurate terms to the effect that the solution is always accurate over a wide range of time. An example will be given later to verify this point.

For the solution of the interface positions at the second stage when $t_1 < t \leqslant P$, i and m in (33) are taken to be 2 and 1, respectively. Further, setting $x = R_1(t)$ and $T(R_1(t), t) = 0$ in (33) yields

$$\sum_{n=1}^{N_2} \left\{ \frac{dR_1(t_n^-)}{dt} \int_{\tau=t_{n-1}}^{t_n} G(R_1(t_{N_2}), t_{N_2} | R_1(\tau), \tau)\, d\tau \right\} - \sum_{n=N_1+1}^{N_2} \left\{ \frac{dR_2(t_n^-)}{dt} \int_{\tau=t_{n-1}}^{t_n} G(R_1(t_{N_2}), t_{N_2} | R_2(\tau), \tau)\, d\tau \right\} = \frac{c}{L} T_0(R_1(t_{N_2}), t_{N_2}). \quad (37)$$

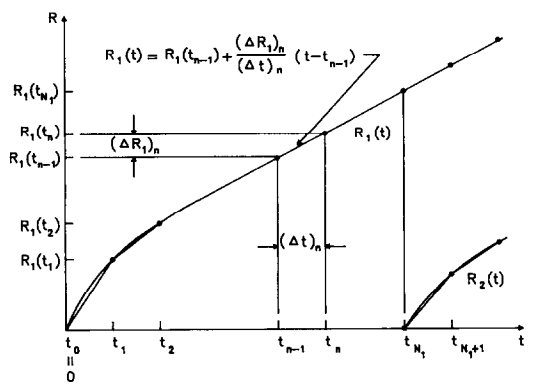

FIG. 3. Linearization of the interface position curve for numerical solution.

In a similar fashion, setting $x = R_2(t)$ and $T(R_2(t), t) = 0$ yields

$$\sum_{n=1}^{N_2} \left\{ \frac{dR_1(t_n^-)}{dt} \int_{\tau=t_{n-1}}^{t_n} G(R_2(t_{N_2}), t_{N_2} | R_1(\tau), \tau)\, d\tau \right\} - \sum_{n=N_1+1}^{N_2} \left\{ \frac{dR_2(t_n^-)}{dt} \int_{\tau=t_{n-1}}^{t_n} G(R_2(t_{N_2}), t_{N_2} | R_2(\tau), \tau)\, d\tau \right\} = \frac{c}{L} T_0(R_2(t_{N_2}), t_{N_2}) \quad (38)$$

where $t_0 = 0$; $R_2(t_{N_1}) = 0$; $N_2 = N_1 + 1, N_1 + 2, \ldots, N_2$; $t_1 < t_{N_2} \leqslant P$. Equations (37) and (38) will be solved simultaneously for dR_1/dt and dR_2/dt. In this effort, the position R and its gradient dR/dt are related as shown in Fig. 3. The position R should thus be discounted as an unknown. Equations (36)–(38) contain convolution integrals; the interface positions must therefore be determined at the N values sequentially chosen.

Once the interface positions are found, they can be used in (33) to find $T(x, t)$. Finally, the cumulative heat input at the surface can be determined by using

$$\int_0^{t_n} q(t)\, dt = \rho(-1)^{m-1} \int_0^{R_1(t_n)} [L + cT(x, t_n)]\, dx \quad (39)$$

for $0 \leqslant t_n \leqslant t_1$, and

$$\int_0^{t_n} q(t)\, dt = \rho(-1)^m \left\{ \int_0^{R_2(t_n)} L\, dx - \int_0^{R_1(t_n)} [L + cT(x, t_n)]\, dx \right\} \quad (40)$$

for $t_1 < t_n \leqslant P$. They are derived strictly on the basis of energy considerations. Their formats permit the separation of the latent heat from the sensible heat, an important part of study for the Stefan problem. The solution is now complete.

UNIQUENESS, CONVERGENCE, ACCURACY AND STABILITY

The interface position is unique, which can be proved by using equation (36). Notice that a graphical determination of the interface position would require plotting both sides of this equation along the y axis with R on the x axis in the same coordinate; the interface position can then be found by locating the point of intersection of the curves. It can be shown that these curves are continuous and monotonic. There is only one point of intersection, a necessary condition for a unique solution [49].

The numerical solution presented in this paper converges, and is accurate and stable as tested by using two examples. The first example deals with a one-phase melting of aluminum whose boundary is imposed with a time-variant exponential condition given by the relation

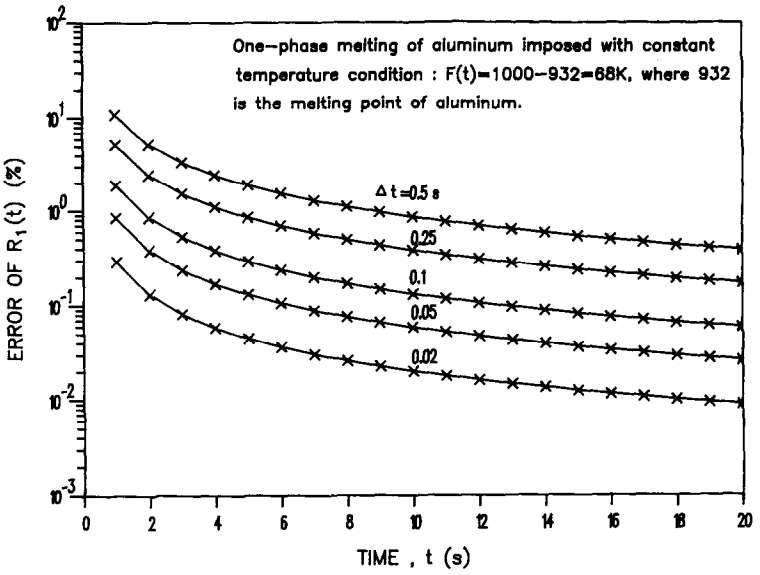

FIG. 4. Accuracy, convergence, and stability tests of the Stefan problem imposed with the constant temperature condition.

$$F(t) = \frac{L}{c}\left[\exp\left(\frac{s^2 t}{\alpha}\right) - 1\right] \tag{41}$$

where s can be shown to represent the speed of the interface motion. This problem is often considered as physically insignificant in the literature yet can be solved exactly. Equation (41) is equivalent to imposing a time-variant flux condition

$$G(t) = \rho s L \exp\left(\frac{s^2 t}{\alpha}\right). \tag{42}$$

Thus the same example provides testing not only of the accuracy of the results but the derivation in the solution as well. For the present paper, a bisection method is used to find the interface position using (36) in which the convergence criterion is taken to be 3×10^{-16}, and the results (not shown) indicate that the errors are less than 0.05%, which is found at small time and with a time increment Δt as large as 0.25 s. This good result can be ascribed to the fact that, for the exponential conditions given in (41) and (42), the interface position varies linearly with time. No error is thus introduced by moving $dR_1(t_n^-)/dt$ out of the integral in (36).

The second example deals with a one-phase melting of aluminum imposed with a constant temperature condition. Commonly known as the Stefan–Neumann problem, it is amenable to an exact solution in which the interface position has a distinct curvature at small time. This problem provides a test of accuracy due to this curvature. As shown in Fig. 4, the interface position converges with the use of small time increments. Even with an increment as large as 0.1 s, the error diminishes below 0.1% at large time. More important, the error does not grow as in other time marching schemes but is suppressed with the advance of time, a unique feature discussed in the previous section and in great detail in refs. [49, 52]. This completes the tests of convergence, accuracy, and stability of the solution.

ILLUSTRATIVE EXAMPLES

Two examples are used to show the temperature distribution, heat exchange, and interface positions in a phase-change material imposed with cyclic temperature and flux conditions given as

$$F(t) = 932 + 200 \sin\left(\frac{\pi}{10} t\right) (\mathrm{K}) \tag{43}$$

$$G(t) = 3 \times 10^6 \sin\left(\frac{\pi}{10} t\right) (\mathrm{W\,m^{-2}}) \tag{44}$$

where the period is 20 s. Aluminum is again used for tests, which has a modified Stefan number (cT_m/L) of 2.27 [52]. Only one cycle is tested for both examples, and the time increment used is taken to be 0.05 s. As before, a bisection method with the same convergence criterion is employed to find the interface position. Based on the tests with the Stefan–Neumann problem in the previous section and the curvature of the interface positions in the present investigation, the error in the positions is estimated to be less than 0.1%. Notice that, for the flux condition given by (44), the overall heat input over the cycle must be zero, a requirement that can be tested for the overall accuracy in the computation as shown in the next section.

RESULTS AND DISCUSSION

Cyclic temperature condition

The interface positions for the cyclic temperature condition are plotted in Fig. 5. Here two curves are

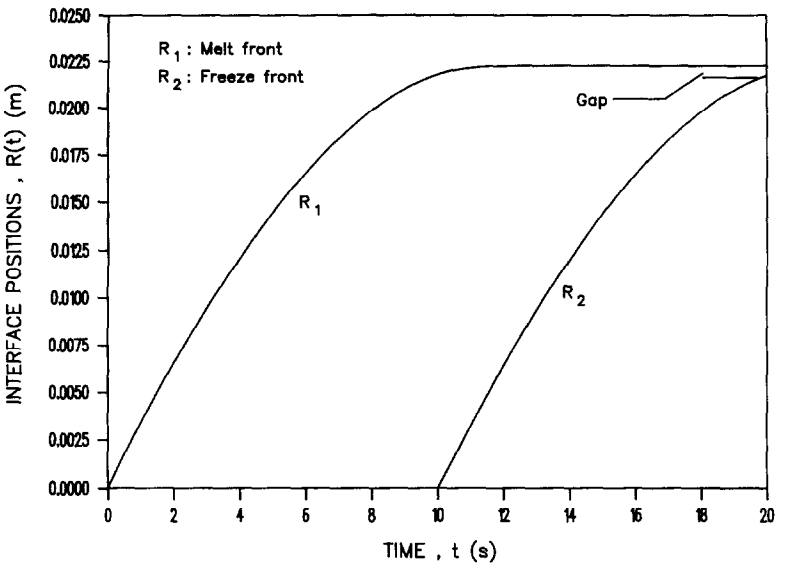

FIG. 5. Interface position curves for a Stefan problem imposed with the cyclic temperature condition.

shown; R_1 represents the melting front, while R_2 represents the freezing front. A close examination of these curves shows that the melting front continues to advance even though the surface starts to re-freeze. This can be ascribed to the fact that, in (16), R_1 is stationary only when the slope of the temperature curve at the melt front is zero. This slope, however, is not zero, as will be shown later. Another point of interest is that if the R_2 curve is moved horizontally to the left so that it matches the R_1 curve at the origin, then the R_2 curve would lie right underneath the R_1 curve, signifying that the freeze front lags slightly behind the melt front. Again this can be explained by referring to the temperature profiles as will now be discussed.

The temperature profiles in the aluminum are shown in Figs. 6 and 7. Figure 6 covers times from 1 to 5 s and 11 to 15 s. These times cover the rapid temperature rise and drop parts of the HIP and HOP. Putting them in one figure permits comparison of the temperature profiles during the corresponding heating and cooling parts of the cycle. This leaves the rest of the temperature curves to be placed in Fig. 7; here again they cover the corresponding cooling and heating parts of the cycle. It is noted that, in these figures, the interface positions can be identified by locating the point of intersection of the curves with the x axis at zero temperature. Then, according to Fig. 6, the freeze-front positions always lie slightly to the left of the melt-front positions, indicating that the freeze front lags behind the melt front. This freeze delay may be attributed to the temperature profile in the melt region at 10 s (see Fig. 7). Here, because of the sensible heat stored in the melt region, a portion of the heat removed from the surface after this time is used to remove this sensible heat; whereas at time greater than zero, heat is added to a medium that is initially at zero temperature. More heat thus goes to melting, resulting in a faster melting front. There is a slope of the temperature curve at the melting front at 10 s; this slope contributes to the continuous motion of the front, as mentioned earlier. Of particular interest is the appearance of the small section of the temperature curve lying above the x axis at 11 s (Fig. 6). This provides further evidence of the importance of the sensible heat and the delay of the freeze front. The freeze front will eventually merge with the melt front, but this will occur shortly after the start of the second cycle, which is not analyzed in this paper.

One application of the phase-change material is to use it for energy storage. It is thus important to examine how the heat is stored in different phases of the medium. Use is made of the cumulative and instantaneous heat histories shown in Figs. 8 and 9, respectively. Figure 8 is plotted using equations (39) and (40), whereas Fig. 9 is plotted by computing the difference of the Q at t_n and t_{n-1} and dividing it by $(t_n - t_{n-1})$; the result is then taken to be the instantaneous heat at $t_{n-1/2}$. Referring to these figures provides insight into how the heat is stored in the medium.

Clearly the shape of the latent heat curve is the result of the motion of the phase-change fronts. During HIP, the melt front slows down with the advance of time, resulting in a drop of the latent heat that is instantaneously stored (Fig. 9) and the decline of the slope of the cumulative latent heat curve with time (Fig. 8). Moving into HOP, the latent heat is released; here because of the sensible heat stored in the melt region at 10 s, the instantaneous heat released at 10.5 s is smaller than that stored at 0.5 s. Otherwise, the latent heat release curve follows the heat store curve in Fig. 8 but in an inverted fashion. Notice that there is a small amount of latent heat cumulatively stored at the end of the cycle, and this is due to the gap

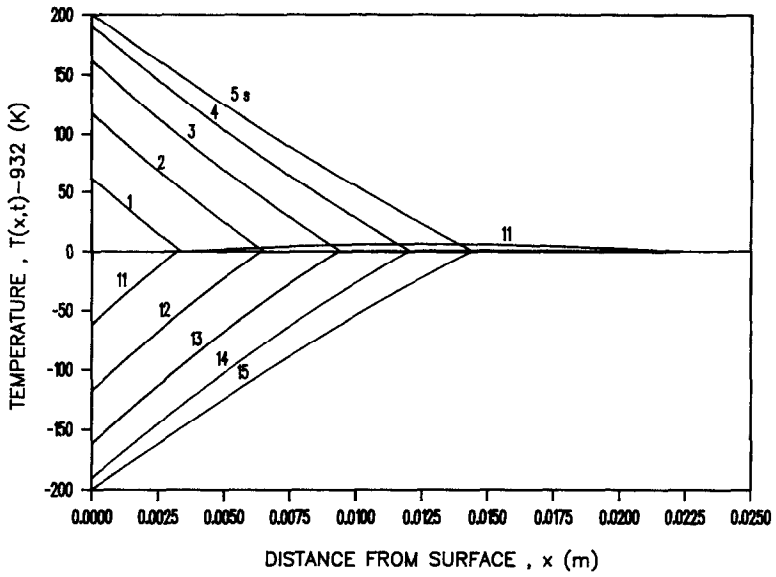

FIG. 6. Temperature profiles for 1–5 and 11–15 s for a Stefan problem imposed with the cyclic temperature condition.

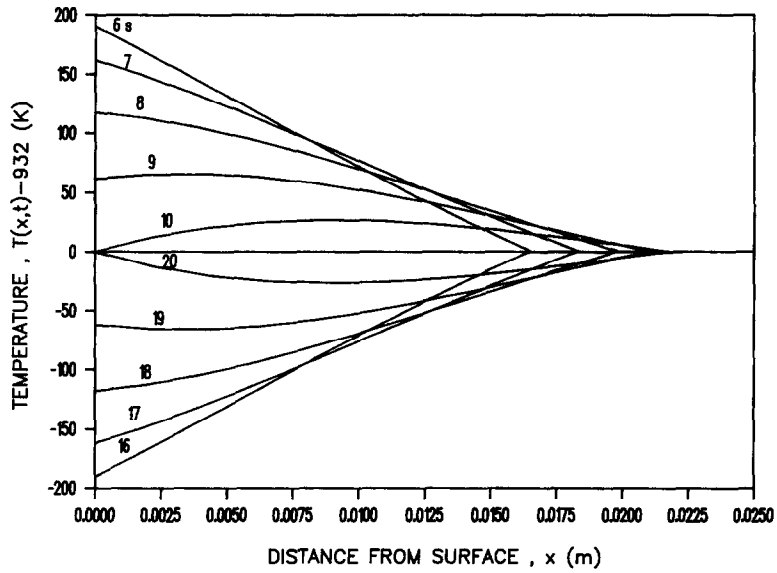

FIG. 7. Temperature profiles for 6–10 and 16–20 s for a Stefan problem imposed with the cyclic temperature condition.

between the melt front and the freeze front. As mentioned earlier, this gap will eventually be closed moving into the second cycle, then the latent heat will be zero.

The sensible heat stored lags behind the surface temperature imposed (Fig. 8). For example, the surface temperature peaks at 5 s, while the sensible heat cumulatively stored peaks at about 6.5 s. This can be ascribed to the fact that during the initial period of heat input, a large amount of heat is used for phase change, leaving little for sensible gain (see the data near 1 s in Figs. 8 and 9). Notice that the cumulative sensible heat is zero at about 11 s, and the sensible heat curve is cyclic in Fig. 8. The sensible heat is thus negative at 20 s, when it has an absolute value greater than the latent heat stored. There is a net loss of the total heat at the end of the cycle, an outcome which is unexpected. On the other hand, there is great complication of the instantaneous heat curves at 10 s in Fig. 9, and this must be the result of the simultaneous appearance of the melt and freeze fronts at that time. The fact that the latent heat curve is much higher than the sensible heat curve bears a clear testimony of the effectiveness of the latent heat storage. The gap

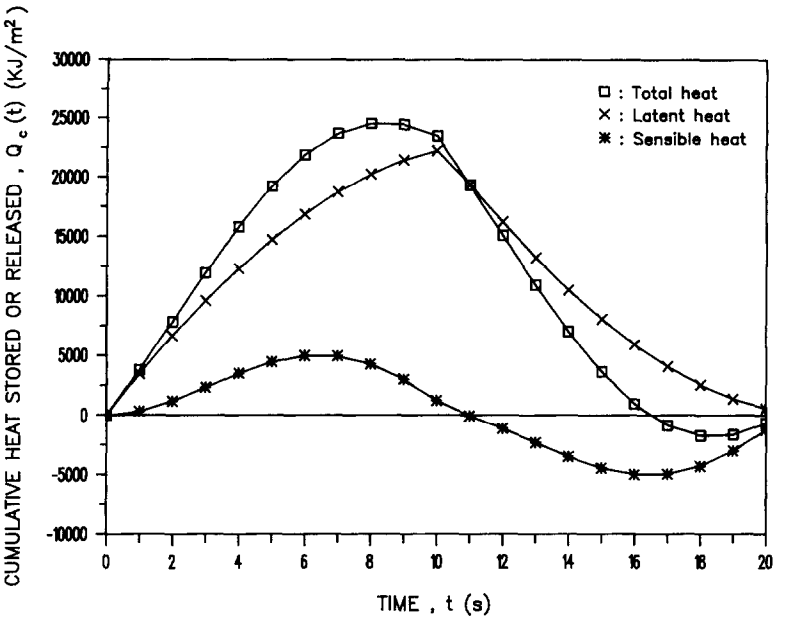

FIG. 8. Cumulative heat histories for a Stefan problem imposed with the cyclic temperature condition.

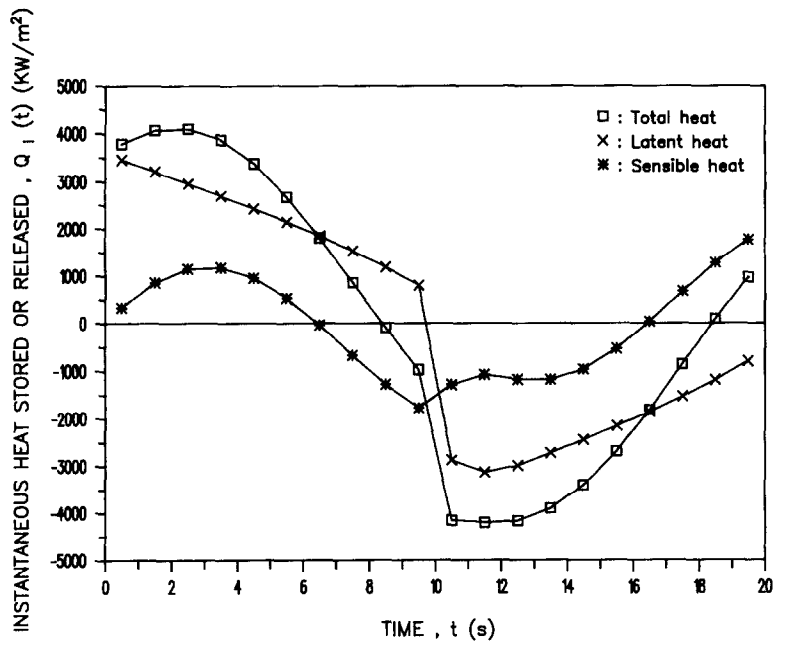

FIG. 9. Instantaneous heat histories for a Stefan problem imposed with the cyclic temperature condition.

between the melt front and the freeze front also contributes to a number of problems associated with material processing and treatment of importance to material scientists.

Cyclic flux condition

A cyclic heat flux input to the medium yields results that are markedly different from those under a cyclic temperature condition. As shown in Fig. 10, the freeze front does not appear until after 11 s, whereas the half period of the flux cycle is 10 s, a delay of about 1 s. Again there is a continuous motion of the melt front after the emergence of the freeze front; however, the freeze front does not travel as far, resulting in a large gap between the melt front and the freeze front at the end of the cycle. Moving the R_2 curve to the left so that it matches the R_1 curve at the origin places the R_2 curve to the left of the R_1 curve; there is a large gap between them, indicating that the freeze front actually moves faster than the melt front.

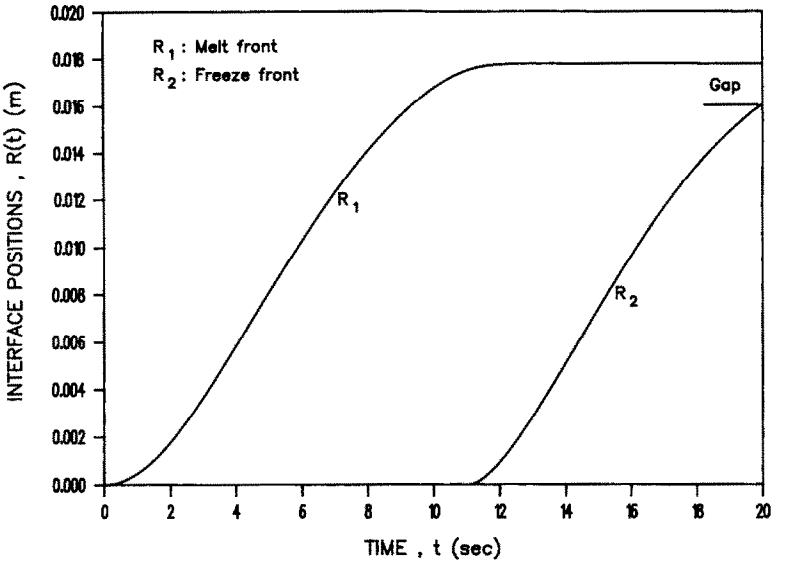

FIG. 10. Interface position curves for a Stefan problem imposed with the cyclic heat flux condition.

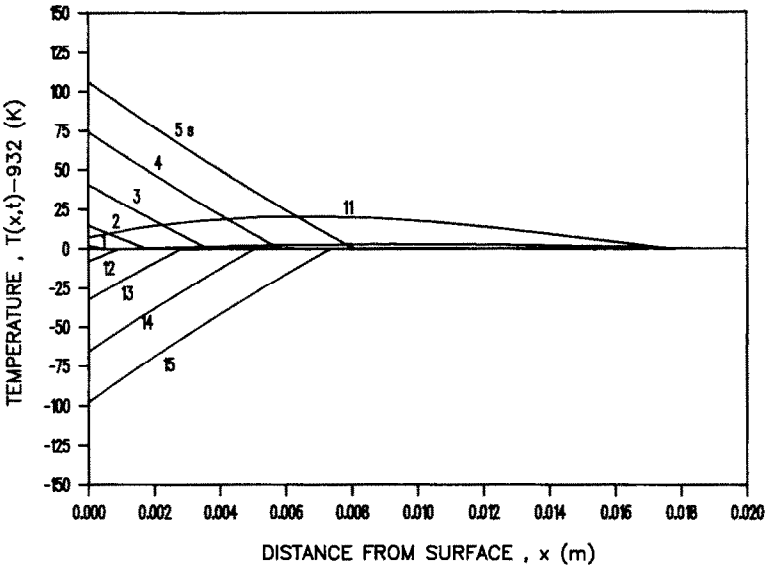

FIG. 11. Temperature profiles for 1–5 and 11–15 s for a Stefan problem imposed with the cyclic heat flux condition.

Two composite temperature plots are again given for the flux condition. The temperature profiles at 1–5 s in Fig. 11 are totally expected. However, for the flux condition, the medium is still in the liquid phase even at 11 s; the temperature curve is above the x axis at zero temperature. There is still an appreciable amount of sensible heat stored at that time. The temperature profile at 12 s resembles that for the temperature cycle at 11 s in Fig. 6—the temperature profile is divided into two parts, one above the x axis, one below the x axis. Comparing the positions of the intersection of the curves with the x axis in Fig. 11 again reveals the delay of the freeze front, which, however, moves faster than the melt front as mentioned earlier. The composite temperature plot given in Fig. 12 indicates that the liquid temperature continues to rise from 6 to 7 s even though the surface flux drops during that time. This phase shift can be better viewed by referring to the surface temperature plot given in Fig. 13.

The cumulative and instantaneous heat stored in the medium are shown in Figs. 14 and 15. Here, the majority of the heat input right after the imposition of the flux condition again goes to the latent heat, which continues to grow (see Fig. 14) even after 10 s. The cumulative sensible heat stored remains cyclic and is out of phase with the input flux cycle given in

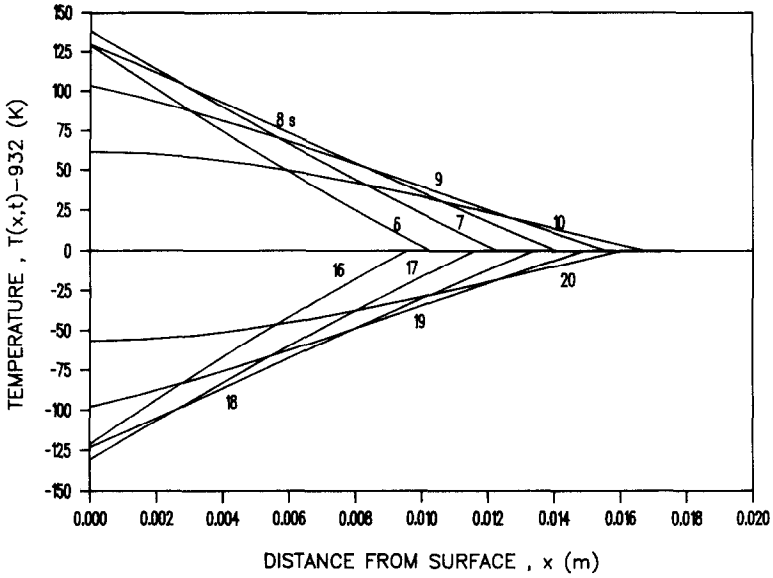

FIG. 12. Temperature profiles for 6–10 and 16–20 s for a Stefan problem imposed with the cyclic heat flux condition.

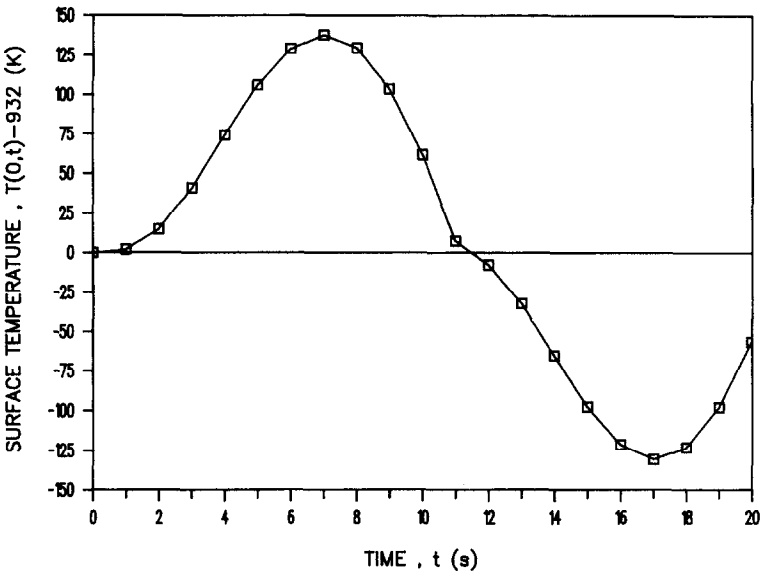

FIG. 13. Surface temperature for a Stefan problem imposed with the cyclic heat flux condition.

Fig. 15 (see the total heat curve there). Of particular interest is the cumulative heat at the end of the cycle (see Fig. 14). Here because of the cyclic flux condition, this total heat must be zero at the end of the cycle. Numerical results show that the cumulative heat stored as latent heat at the end of the cycle is within 99.99% of that withdrawn as sensible heat, giving an indication of the high accuracy of the overall computation in this work.

EXTENSIONS

In the solution developed in this paper, the solid and liquid properties have been treated as being equal. Different property values can be accounted for by using double sources and sinks as shown in ref. [24] and discussed in great detail in ref. [25]. It is expected that, with density differences accounted for in a cyclic temperature or flux condition, complicated suction or blowing will occur at the interfaces, thus adding great complexity to the analysis.

It should be stressed that, while only one cycle each of the temperature and flux condition has been analyzed in this work, the method developed is general and applicable to multiple cycles. In such problems, (33) will be used directly if the medium is imposed with a temperature condition. In tracking the interface positions, the left hand side of this equation is set to zero; then, if only one interface appears in the

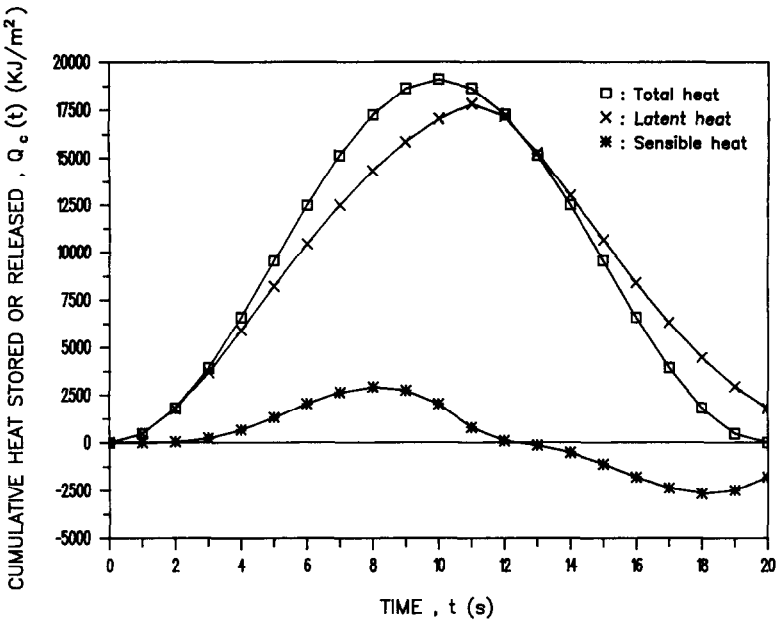

FIG. 14. Cumulative heat histories for a Stefan problem imposed with the cyclic heat flux condition.

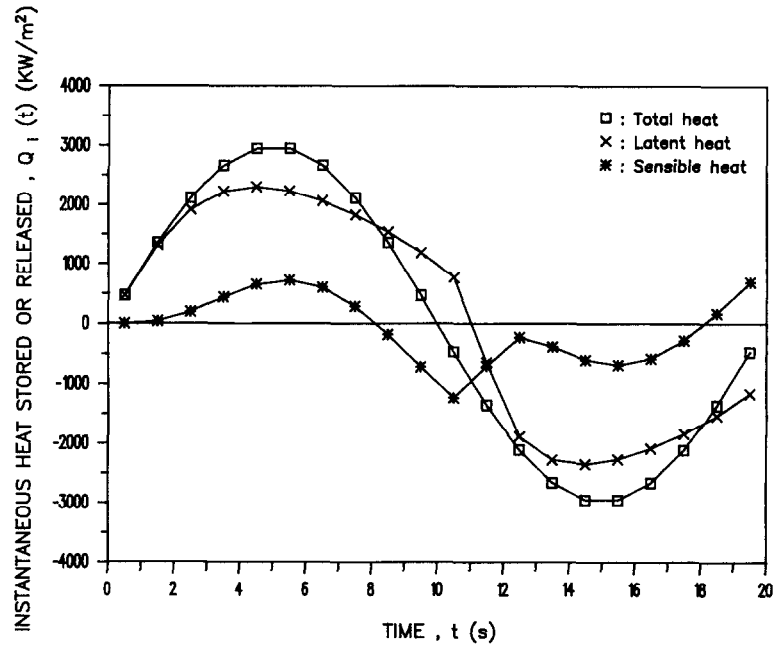

FIG. 15. Instantaneous heat histories for a Stefan problem imposed with the cyclic heat flux condition.

medium, I is set to unity and x is set to $R_1(t)$. The resulting numerical equation is (36). If two interfaces appear in the medium, I is set to 2 and x is set to $R_1(t)$ and $R_2(t)$ as shown in the numerical equations (37) and (38). This process continues for any number of interfaces in the medium. On the other hand, for a cyclic flux condition imposed on the boundary, the surface will generally not re-freeze (or re-melt) halfway through the cycle. Then t_t must be determined prior to the computation of the interface positions. These transition times can be determined by changing x and t in (33) to zero and t_t, respectively. Subsequently, the left hand side of this equation is set to zero to account for the phase change temperature. A special case is provided in (28b), which is solved implicitly for t_t. Other transition times can be evaluated accordingly. Algorithms can thus be developed for handling these multiple cycle situations.

CONCLUDING REMARKS

The present source-and-sink method orginates from the Green function method. However, it is fundamentally different from the way the Green function was used in the development of the boundary element method [53–55]. As compared in ref. [49], the present method is far more accurate than the boundary element method. The present method has thus been applied to the solution of phase change in paraffin wax with subcooling and superheating. For such a problem, there are four stages of temperature in the medium, and the cyclic temperature condition generates melt and freeze fronts that re-combine towards the end of one cycle. An interesting phenomenon related to the hysteresis of energy storage and release is also found as reported in refs. [49, 56].

REFERENCES

1. H. S. Carslaw and J. C. Jaeger, *Conduction of Heat in Solids* (2nd Edn). Oxford University Press, London (1959).
2. J. C. Muehlbauer and J. E. Sunderland, Heat conduction with freezing or melting, *Appl. Mech. Rev.* **18,** 951–959 (1965).
3. T. R. Goodman, Application of integral methods to transient nonlinear heat transfer, *Adv. Heat Transfer* **1,** 71–79 (1964).
4. L. I. Rubinstein, The Stefan problem, *Am. Math. Soc. Transl. Math. Monogr.* 27 (1971).
5. J. R. Ockendon and W. R. Hodgkins, *Moving Boundary Problems in Heat Flow and Diffusion.* Clarendon Press, London (1975).
6. D. G. Wilson, A. D. Solomon and P. T. Boggs, *Moving Boundary Problems.* Academic Press, New York (1978).
7. J. Crank, *Free and Moving Boundary Problems.* Clarendon Press, London (1984).
8. J. M. Hill, *One-dimensional Stefan Problems: an Introduction.* Longman Scientific and Technical, London (1987).
9. L. S. Yao and J. Prusa, Melting and freezing, *Adv. Heat Transfer* **19,** 1–95 (1989).
10. G. W. Evans, E. Isaacson and J. K. L. MacDonald, Stefan-like problems, *Q. Appl. Math.* **8,** 312–319 (1950).
11. L. N. Tao, On free boundary problems with arbitrary initial and flux conditions, *J. Appl. Math. Phys.* **30,** 416–426 (1979).
12. L. N. Tao, Free boundary problems with radiation boundary conditions, *Q. Appl. Math.* **37,** 1–10 (1979).
13. L. N. Tao, The exact solutions of some Stefan problems with prescribed heat flux, *J. Heat Transfer* **48,** 732–736 (1981).
14. S. H. Cho and J. E. Sunderland, Approximate temperature distribution for phase change of a semi-infinite body, *J. Heat Transfer* **103,** 401–403 (1981).
15. J. L. Duda and J. S. Vrentas, Perturbation solutions of diffusion-controlled moving boundary problems, *Chem. Engng Sci.* **24,** 461–470 (1969).
16. R. I. Pedroso and G. A. Domoto, Inward spherical solidification-solution by the method of strained coordinates, *Int. J. Heat Mass Transfer* **16,** 1037–1043 (1973).
17. R. I. Pedroso and G. A. Domoto, Exact solution by perturbation method for planar solidification of a saturated liquid with convection at the wall, *Int. J. Heat Mass Transfer* **16,** 1816–1819 (1973).
18. D. S. Riley, F. T. Smith and G. Poots, The inward solidification of spheres and circular cylinders, *Int. J. Heat Mass Transfer* **17,** 1507–1516 (1974).
19. S. Weinbaum and L. M. Jiji, Singular perturbation theory for melting or freezing in finite domains not at the fusion temperature, *J. Appl. Mech.* **44,** 25–30 (1977).
20. L. M. Jiji and S. Weinbaum, Perturbation solutions for melting or freezing in annular regions initially not at the fusion temperature, *Int. J. Heat Mass Transfer* **21,** 581–592 (1978).
21. Ch. Charach and P. Zolgin, Solidification in a finite, initially overheated slab, *Int. J. Heat Mass Transfer* **28,** 2261–2268 (1985).
22. N. Tokuda, An asymptotic, large time solution of the convection Stefan problem with surface radiation, *Int. J. Heat Mass Transfer* **29,** 135–143 (1986).
23. N. M. H. Lightfoot, Solidification of molten steel, *Proc. Lond. Math. Soc.* **31,** 97–116 (1929).
24. I. I. Kolodner, Free boundary problem for the heat equation with applications to problems of change of phase, *Commun. Pure Appl. Math.* **9,** 1–31 (1956).
25. L. N. Tao, A method for solving moving boundary problems, *SIAM Appl. Math.* **46,** 254–264 (1986).
26. B. A. Boley, The embedding technique in melting and solidification problems, *Moving Boundary Problems in Heat Flow and Diffusion, Proc. Conf. Univ. Oxford,* 25–27 March, pp. 150–172 (1974).
27. J. L. Duda, M. F. Malone, R. H. Notter and J. S. Vrentas, Analysis of two-dimensional diffusion-controlled moving boundary problems, *Int. J. Heat Transfer* **18,** 901–910 (1975).
28. E. M. Sparrow, S. Ramadhyani and S. V. Patankar, Effect of subcooling on cylindrical melting, *J. Heat Transfer* **100,** 395–402 (1978).
29. T. Saitoh, Numerical method for multidimensional freezing problems in arbitrary domains, *J. Heat Transfer* **100,** 294–299 (1978).
30. J. M. Hill and A. Kucera, Freezing a saturated liquid inside a sphere, *Int. J. Heat Mass Transfer* **26,** 1631–1637 (1983).
31. L. S. Yao, Analysis of heat transfer in slightly eccentric annuli, *J. Heat Transfer* **102,** 279–284 (1980).
32. R. M. Furzeland, A comparative study of numerical methods for moving boundary problems, *J. Inst. Math. Applic.* **26,** 411–429 (1980).
33. L. S. Yao and W. Cherney, Transient phase-change around a horizontal cylinder, *Int. J. Heat Mass Transfer* **24,** 1971–1984 (1981).
34. M. Prud'homme, T. H. Nguyen and D. L. Nguyen, A heat transfer analysis for solidification of slabs, cylinders, and spheres, *J. Heat Transfer* **111,** 699–705 (1989).
35. A. Kassinos and J. Prusa, Effects of density change and subcooling on the melting of a solid in a rectangular enclosure, *Proc. 8th Int. Heat Transfer Conf.*, San Francisco, Vol. 4, pp. 1787–1792 (1986).
36. G. E. Bell, Solidification of a liquid about a cylindrical pipe, *Int. J. Heat Mass Transfer* **22,** 1681–1686 (1979).
37. V. J. Lunardini, Phase change around a circular cylinder, *J. Heat Transfer* **103,** 598–600 (1981).
38. W. E. Steward and K. L. Smith, Inward solidification of water in a cylinder—An analytical and experimental study, *ASME/AIChE 23rd Natn. Heat Transfer Conf.*, Denver, 4–7 August, 85-HT-2 (1985).
39. V. D. Rao and P. K. Sarma, Direct contact heat transfer in spherical geometry associated with phase transformation—a closed-form solution, *Int. J. Heat Mass Transfer* **28,** 1956–1958 (1985).
40. J. Mennig and M. N. Ozisik, Coupled integral equation approach for solving melting or solidification, *Int. J. Heat Mass Transfer* **28,** 1481–1485 (1985).
41. R. M. Cotta, M. N. Ozisik and J. Mennig, Coupled integral equation approach for solving phase-change problems in a finite slab, *J. Franklin Inst.* **327,** 225–234 (1990).

42. Z. Dursunkaya and S. Nair, A moving boundary problem in a finite domain, *J. Appl. Mech.* **57,** 50–56 (1990).
43. N. Zabaras, S. Mukherjee and O. Richmond, An analysis of inverse heat transfer problems with phase changes using an integral method, *J. Heat Transfer* **110,** 554–560 (1988).
44. P. K. Banerjee and R. P. Shaw, Boundary element formulation for melting and solidification problems. In *Developments in Boundary Element Methods*—2 (Edited by P. K. Banerjee and R. P. Shaw), pp. 1–18. Barking, Essex (1982).
45. K. O'Neill, Boundary integral equation solution for moving boundary phase change problems, *Int. J. Numer. Meth. Engng* **19,** 1825–1850 (1983).
46. M. Heinlein, S. Mukherjee and O. Richmond, A boundary element method analysis of temperature fields and stresses during solidification, *Acta Mech.* **59,** 59–81 (1986).
47. A. M. Sadegh, L. M. Jiji and S. Weinbaum, Boundary integral equation technique with application to freezing around a buried pipe, *Int. J. Heat Mass Transfer* **30,** 223–232 (1987).
48. N. Zabaras and S. Mukherjee, An analysis of solidification problems by the boundary element method, *Int. J. Numer. Meth. Engng* **24,** 1879–1900 (1987).
49. C.-Y. Choi, Exact and numerical solution of one- and two-phase melting and solidification problems imposed with constant or time-variant temperature and flux conditions, Ph.D. dissertation, University of Florida (1991).
50. M. Aramowitz and I. A. Stegun, *Handbook of Mathematical Functions*. Dover, New York (1964).
51. I. S. Gradshteyn and I. M. Ryzhik, *Table of Integrals, Series, and Products*. Academic Press, New York (1980).
52. C. K. Hsieh and C.-Y. Choi, Solution of one- and two-phase melting and solidification problems imposed with constant or time-variant temperature and flux boundary conditions, *J. Heat Transfer* (in press).
53. C. K. Hsieh and C.-Y. Choi, A domain extension method for quantitative detection of cavities by infrared scanning, *J. Nondestruct. Eval.* **8,** 195–211 (1989).
54. A. J. Kassab and C. K. Hsieh, Application of the complex variable boundary element method to solving potential problems in doubly connected domains, *Int. J. Numer. Meth. Engng* **29,** 161–179 (1990).
55. C. K. Hsieh and A. J. Kassab, Complex variable boundary element methods for the solution of potential problems in simply and multiply connected domains, *Comput. Meth. Appl. Mech. Engng* **86,** 189–213 (1991).
56. C. K. Hsieh and C.-Y. Choi, A general analysis of phase change energy storage for solar energy applications, *J. Solar Energy Engng* (in press).

SOLUTIONS DES PROBLEMES DE STEFAN AVEC CONDITIONS AUX LIMITES DE TEMPERATURE ET DE FLUX CYCLIQUES

Résumé—Des problèmes de Stefan avec des conditions aux limites de température et de flux cycliques sont résolus en utilisant des méthodes de source et de puit. Un front-source est associé à un front mobile de solidification tandis qu'un front-puit est associé à un front mobile de fusion. Le problème est exprimé par un système d'équations intégro-différentielles qui est résolu numériquement pour les positions de l'interface, les profils de température, le stockage (ou la libération) de chaleur cumulatif et instantané. Les méthodes de résolution sont montrées être uniques, convergentes, stables et précises. Bien qu'elles sont utilisées comme test sur un cycle de température ou de flux, elles sont générales et applicables à des cycles multiples. Les résultats numériques révèlent des phénomènes intéressants non décrits antérieurement. Leur application au stockage de l'énergie est considérée.

LÖSUNG VON STEFAN-PROBLEMEN BEI RANDBEDINGUNGEN MIT ZYKLISCH SCHWANKENDEN TEMPERATUR- UND WÄRMESTROMDICHTEN

Zusammenfassung—Stefan-Probleme mit zyklisch schwankenden Temperaturen und Wärmestromdichten als Randbedingung werden unter Verwendung der Quellen/Senken-Methode gelöst. Eine Quellenfront ist mit einer beweglichen Gefrierfront, eine Senkenfront mit einer beweglichen Schmelzfront verbunden. Die Lösung wird durch einen Satz gekoppelter Integro-Differentialgleichungen beschrieben, welche numerisch gelöst werden. Dabei ergibt sich der Grenzflächenverlauf, Temperaturprofile sowie Summen- und Momentanwerte für die gespeicherte und abgegebene Wärme. Obwohl die entwickelten Verfahren mit nur jeweils einer Randbedingung für Temperatur und Wärmestromdichte überprüft worden sind, sind sie doch allgemeingültig und auf mehrfache Zyklen anwendbar. Die numerischen Ergebnisse zeigen interessante Phänomene, welche bisher in der Literatur noch nicht beschrieben worden sind. Außerdem wird ihre Bedeutung für die Energiespeicherung sowie die Materialentwicklung und-behandlung diskutiert.

РЕШЕНИЕ ЗАДАЧИ СТЕФАНА С ЦИКЛИЧЕСКИМИ ГРАНИЧНЫМИ УСЛОВИЯМИ ДЛЯ ТЕМПЕРАТУРЫ И ТЕПЛОВОГО ПОТОКА

Аннотация—Задачи Стефана с циклическими граничными условиями для температуры и теплового потока решаются методами источника и стока. Фронт источника связан с движущимся фронтом замерзания, в то время как фронт стока связан с движущимся фронтом плавления. Решение выражено системой связанных интегродифференциальных уравнений, которые решаются численно для определения положения границы раздела, профилей температуры и суммарного и Мгновенного значений количества аккумулированного и выделенного тепла. Показано, что методы решения являются уникальными, сходящимися, устойчивыми и точными. Несмотря на то, что предложенные методы используются для испытания одного цикла каждого из условий температуры и потока, они являются общими и могут применяться к многократным циклам. Численные результаты отражают интересные явления, ранее не отмечавшиеся в литературе. Рассмотрено также их отношение к проблеме накопления энергии и обработки материалов.